DIGITAL COMPUTER SOLUTIONS FOR EXCITATION AND PROPAGATION OF THE NERVE IMPULSE

J. W. COOLEY *and* F. A. DODGE, JR.
From the IBM Watson Research Center, Yorktown Heights, New York

ABSTRACT The Hodgkin-Huxley model of the nerve axon describes excitation and propagation of the nerve impulse by means of a nonlinear partial differential equation. This equation relates the conservation of the electric current along the cablelike structure of the axon to the active processes represented by a system of three rate equations for the transport of ions through the nerve membrane. These equations have been integrated numerically with respect to both distance and time for boundary conditions corresponding to a finite length of squid axon stimulated intracellularly at its midpoint. Computations were made for the threshold strength-duration curve and for the repetitive firing of propagated impulses in response to a maintained stimulus. These results are compared with previous solutions for the space-clamped axon. The effect of temperature on the threshold intensity for a short stimulus and for rheobase was determined for a series of values of temperature. Other computations show that a highly unstable subthreshold propagating wave is initiated in principle by a just threshold stimulus; that the stability of the subthreshold wave can be enhanced by reducing the excitability of the axon as with an anesthetic agent, perhaps to the point where it might be observed experimentally; but that with a somewhat greater degree of narcotization, the axon gives only decrementally propagated impulses.

INTRODUCTION

Hodgkin and Huxley (1952) have formulated a complete mathematical model of the squid axon which can be solved to describe excitation and propagation of the nerve impulse. In this model, the total membrane current (I_m) at any point along the axon is given by the sum of the displacement current of the membrane capacitance ($C \cdot dV/dt$) and the current carried by the movement of ions through the membrane (I_i). From their analysis of voltage-clamp measurements, they showed that the ionic current could be resolved into two major components, one carried by sodium ions, the other by potassium. Each component was found to be linearly proportional to its respective electrochemical driving force. But the proportionality constants, the specific sodium and potassium ionic conductances, were found to be

highly nonlinear functions of the membrane potential and of time. In the absence of detailed knowledge of the molecular dynamics of the membrane, the functional dependence of the conductances was described empirically by a system of first-order rate equations. The complete model for the axon is then obtained by inserting the equations for I_m at any point into an appropriate equation for the conservation of current along the axon.

In general, the distribution of membrane current in a uniform unmyelinated axon is described by the partial differential equation for a one dimensional cable; i.e.,

$$\frac{a}{2R}\frac{\partial^2 V}{\partial x^2} = I_m = C\frac{\partial V}{\partial t} + I_i. \tag{1}$$

Previous applications of the model to the squid axon have been restricted to either of two constraints upon the cable equation which simplify the complete model to a system of ordinary differential equations. By appropriate experimental procedures the membrane potential can be constrained to have the same value along a finite length of axon (space-clamp constraint). Hence, equation (1) is simplified to

$$I_m = C\frac{dV}{dt} + I_i \tag{2}$$

Under this condition the model predicted the waveform of the membrane action potential, subthreshold responses, the time course of the membrane conductance change, refractoriness, and the net exchange of sodium and potassium ions (Hodgkin and Huxley, 1952), which agreed well with independent experimental measurements. Subsequently, the space-clamp model has been solved for the threshold strength-duration curve and repetitive firing (Cole et al., 1955; FitzHugh and Antosiewicz, 1959) to account for the effect of the calcium ion concentration on excitability (Huxley, 1959*a*) and to investigate the theoretical behavior near threshold (FitzHugh, 1961). The alternative constraint on equation (1) is obtained by assuming that the propagating nerve impulse is a uniform wave, i.e. $V(x, t) = V(x - \theta t)$, where θ is the conduction velocity. Hence, equation (1) is simplified to

$$\frac{a}{2R\theta^2}\frac{d^2 V}{dt^2} = C\frac{dV}{dt} + I_i. \tag{3}$$

By a laborious trial and error procedure, Hodgkin and Huxley (1952) found a value of θ which yielded a solution to equation (3) and this solution predicted a waveform of the normal propagating impulse and its velocity in good agreement with experimental measurements. In a later theoretical investigation Huxley (1959*b*) found that there exist two other solutions of equation (3), corresponding to a single subthreshold wave and an indefinitely long train of subthreshold oscillations, which propagate much more slowly than the normal impulse. Presumably, such subthreshold waves would be very unstable and perhaps not observable in an experiment.

The initiation of propagated impulses in an unconstrained axon can be examined theoretically only by solving the partial differential equation (1). FitzHugh (1962) has treated the special case of the vertebrate myelinated axon, in which regeneration of the propagating impulse takes place at discrete points (the nodes of Ranvier) well separated along an otherwise passive cable. Each node was represented by appropriate scaling of the Hodgkin-Huxley equations on the basis of the essential similarity of the current-voltage relations of a node and the squid axon (Dodge and Frankenhaeuser, 1958). Solution of this model accurately described the initiation and saltatory conduction of the impulse in the myelinated fiber. However, because of the fundamental differences in cable structure, these results are not directly applicable to the continuous unmyelinated axon.

We have programmed the IBM 7094 computer to solve the nonlinear partial differential equation of the Hodgkin-Huxley model for the squid axon. With such solutions we haxe examined some of the classical excitation phenomena and have investigated the stability properties of the subthreshold propagating waves.

EQUATIONS

For these computations we have considered a long uniform axon, bathed by a large volume of sea water, and stimulated with an intracellular microelectrode at its midpoint. The lumped equivalent circuit corresponding to these conditions is shown in Fig. 1.

In a large volume, the external longitudinal resistance is negligible in comparison with the internal. The axon is divided into numerous segments, δx in length, sufficiently short that the membrane potential (V) can be considered uniform over a segment. The membrane characteristics are represented by the Hodgkin-Huxley ordinary (space-independent) differential equations scaled to the area of a segment. Adjacent segments are connected by a resistance $r\delta x$, where r is internal resistance per unit length.

An appropriate finite difference approximation to the partial differential equation (1) is conveniently derived from this equivalent circuit. For any segment, except the one at the stimulating electrode ($x = 0$), the total membrane current (i_m) must be equal to the difference between the longitudinal current which enters from the left and that which leaves to the right; i.e.,

$$i_m = (V_{i-1} - V_i/r\delta x) - (V_i - V_{i+1}/r\delta x). \quad (4)$$

This equation is normalized to membrane current density by the relations $I_m = i_m/2\pi a\delta x$ and $r = R/\pi a^2$, yielding

$$I_{m_j} = \frac{a}{2R} \cdot \frac{V_{j-1} - 2V_j + V_{j+1}}{(\delta x)^2}, \qquad (j = 1, 2, 3 \cdots J). \quad (5)$$

For the boundary conditions at the stimulating electrode ($x = 0$), $i_m = I_s + (V_{-1} - V_0/r\delta x) - (V_0 - V_1/r\delta x)$. The assumed conditions imposed symmetry

with respect to $x = 0$; i.e., in general $V_{-j} = V_j$. Applying this symmetry condition and normalizing as above, yields

$$I_{m_0} = \frac{1}{\delta x}\left[\frac{I_s}{2\pi a} - \frac{a}{R}\frac{(V_0 - V_1)}{\delta x}\right], \qquad (j = 0). \tag{6}$$

For the boundary condition at the end of the axon, we simply assume

$$V_{J+1} \equiv 0. \tag{7}$$

With this rather unrealistic assumption we avoid computing the spread of depolarization from the cut end of the axon. However, we do not avoid the distortion of the longitudinal current as an impulse approaches the end; hence, the computations were carried out for an axon at least a centimeter longer than the spatial dimension of interest.

The mathematical model is summarized by the following equations (Hodgkin and Huxley, 1952). [Note, in conformity with recent practice, the sign convention for current and potential is taken here in the sense opposite to that used by Hodgkin and Huxley.] The variables and constants are defined in the *Key to Abbreviations.*

KEY TO ABBREVIATIONS

Variables:

t = time (msec)
$x_j = j\delta x$ = distance along axon (cm) from stimulating electrode
$V_j(t)$ = membrane potential (mv), measured in the sense of internal minus external potential, with the zero of potential scale arbitrarily assigned to the resting potential, at the j^{th} segment
$I_{m_j}(t)$ = total membrane current density (μa/cm^2) at the j^{th} segment
$I_{i_j}(t)$ = ionic current density (μa/cm^2) at the j^{th} segment
I_s = amplitude of the stimulating current (μa) at $x = 0$
m_j, h_j, n_j = HH conductance variables (dimensionless) at the j^{th} segment

Constants (standard values):

a = radius of axon (0.0238 cm)
R = specific resistance of axoplasm (34.5 ohm cm)
C = specific membrane capacitance (1 μf/cm^2)
$\bar{g}_{Na}$ = maximum sodium conductance (120 mmho/cm^2)
V_{Na} = sodium equilibrium potential (+115 mv)
$\bar{g}_K$ = maximum potassium conductance (36 mmho/cm^2)
V_K = potassium equilibrium potential (−12 mv)
g_L = nonspecific leakage conductance (0.3 mmho/cm^2)
V_L = equilibrium potential of leakage current (+10.598 mv)

Dot notation is used to denote differentiation with respect to time. Equation (8) describes the conservation of the capacitative, local circuit and ionic currents at any point. Equation (9) relates the local value of the ionic current to the specific ionic conductances and the respective electrochemical driving forces. Equations (10),

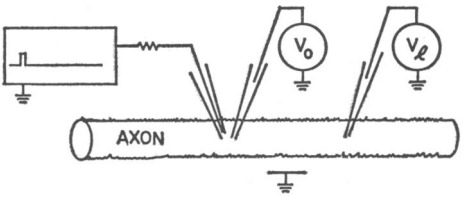

APPROXIMATION OF THE PARTIAL DIFFERENTIAL EQUATION

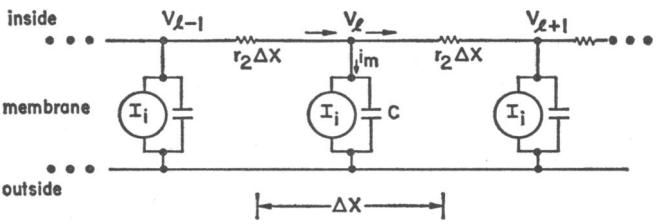

FIGURE 1 Lumped equivalent circuit representing a continuous axon under conditions described in text.

(11), and (12) empirically describe the functional dependence of the ionic conductances upon the local value of the membrane potential.

$$C\dot{V}_j = I_{m_j} - I_{i_j} \qquad (j = 0, 1, 2 \cdots J) \tag{8}$$

$$I_{i_j} = \bar{g}_{Na} m_j^3 h_j (V_j - V_{Na}) + \bar{g}_K n_j^4 (V_j - V_K) + g_L (V_j - V_L) \tag{9}$$

$$\dot{m}_j = \alpha_m (1 - m_j) - \beta_m m_j \tag{10}$$

$$\dot{h}_j = \alpha_h (1 - h_j) - \beta_h h_j \tag{11}$$

$$\dot{n}_j = \alpha_n (1 - n_j) - \beta_n n_j, \tag{12}$$

where I_{m_j} is given by equations (5) and (6). The empirical rate constants (α's and β's) are evaluated for each V, according to the approximating functions given by Hodgkin and Huxley (1952), which are appropriate to this standard temperature of 6.3° C. For any other temperature, all the rate constants are multiplied by the factor ϕ, where $\phi = 3^{T-6.3/10}$. The relatively small temperature dependence of $\bar{g}_{Na}$ and $\bar{g}_K$ (Moore, 1958) has been neglected.

For all calculations the initial conditions corresponded to a uniform resting state; i.e., all $V_j = 0$ and all m_j, h_j, and n_j had their steady-state values for $V = 0$.

NUMERICAL INTEGRATION METHOD

For the integration with respect to time we have used a constant integration step (δt) be-

cause, as long as the potential spike is somewhere on the axon, δt must be small enough to permit an accurate calculation of the rapid changes accompanying it.

For the description of the integration, values of variables at time t_k will have the superscript "k" affixed. The first step is to calculate an approximate set of values of V_i^{k+1} with the open integration formula

$$V_i^{k+1} = V_i^k + \Delta t \dot{V}_i^k \tag{13}$$

using the values of the independent variables at $t = t_k$. Formula (13) could be used with n, m, and h to yield an acceptable solution at the new time level, but, for accuracy and numerical stability, a very small Δt would be required. Instead, closed integration formulas which are numerically stable and give accuracy of high order in Δt are used. The formulas used here are obtained from the trapezoidal rule of integration and may be written

$$V_i^{k+1} = V_i^k + \frac{\Delta t}{2}(\dot{V}_i^k + \dot{V}_i^{k+1}) \tag{14}$$

$$n_i^{k+1} = n_i^k + \frac{\Delta t}{2}(\dot{n}_i^k + \dot{n}_i^{k+1}) \tag{15}$$

with similar equations for m and h. We write the time derivative of V in the form

$$\dot{V}_i = \frac{1}{C}\left\{\frac{a}{2R\Delta x^2}(V_{i-1} - 2V_i + V_{i+1}) - g_i(V_i - U_i)\right\} \tag{16}$$

where

$$\begin{aligned} g &= g_K + g_{Na} + g_L \\ U &= \frac{g_K V_K + g_{Na} V_{Na} + g_L V_L}{g}. \end{aligned} \tag{17}$$

This is substituted for $\dot{V}_i^{k+1}$ in equation (14) and the resulting system of equations is written

$$\begin{aligned} A_0^{k+1} V_0^{k+1} - V_1^{k+1} &= B_0^{k+1} \\ -V_{i-1}^{k+1} + A_i^{k+1} V_i^{k+1} - V_{i+1}^{k+1} &= B_i^{k+1} \\ -V_{J-1}^{k+1} + A_J^{k+1} V_J^{k+1} &= B_J^{k+1} \end{aligned} \tag{18}$$

where

$$\begin{aligned} A_i^{k+1} &= \frac{2R\Delta x^2}{a}\left(\frac{2C}{\Delta t} + g_i^{k+1}\right) + 2 \\ B_i^{k+1} &= \frac{2R\Delta x^2}{a}\left\{C\left(\frac{2}{\Delta t} V_i^k + \dot{V}_i^k\right) + g_i^{k+1} U_i^{k+1} + \frac{I_{ej}}{\Delta x}\right\}, \end{aligned} \tag{19}$$

$I_{ej} = I_e$ if $j = 0$ and $I_{ej} = 0$ otherwise. Substituting for $\dot{n}_i^{k+1}$ in equation (15) and solving for n_i^{k+1} gives

$$n_i^{k+1} = \frac{n_i^k + \frac{\Delta t}{2}\alpha_{ni}^{k+1}}{1 + \frac{\Delta t}{2}(\alpha_{ni}^{k+1} + \beta_{ni}^{k+1})}. \tag{20}$$

Similar equations are obtained for m and h.

The entire numerical procedure for advancing all variables by one time step is as follows:

(*a*) Values of V_j^k, n_j^k, m_j^k, h_j^k, $j = 0, 1, 2, \cdots, J$ at $t = t_k$ are used in equation (16) to evaluate $\dot{V}_j^k$ which is then used in equation (13) to obtain a first approximation to V_j^{k+1}.

(*b*) The α's and β's of the rate equations are calculated with the approximate V_j^{k+1} and used in equation (20) to get approximate values of n_j^{k+1}, m_j^{k+1}, and h_j^{k+1}.

(*c*) The permeabilities are computed from n_j^{k+1}, m_j^{k+1}, and h_j^{k+1} and from these, g_j^{k+1} and U_j^{k+1} and then A_j^{k+1} and B_j^{k+1}, defined by equation (19), are evaluated.

(*d*) The system of equations (18) is solved by the algorithm:

Let $\Gamma_0 = 0, \quad X_0 = 0.$

For $j = 1, 2, \cdots, J$ calculate

$$\Gamma_j = (A_j - \Gamma_{j-1})^{-1}$$

and

$$X_j = \Gamma_j(X_{j-1} + B_j).$$

Let $V_J^{k+1} = X_J.$

For $j = J - 1, J - 2, \cdots, 1$ calculate

$$V_j^{k+1} = X_j - \Gamma_j V_{j+1}^{k+1}.$$

This yields a new set of values of V_j^{k+1}.

(*e*) If the correction to V_j^{k+1} is more than a prescribed convergence criterion, taken here as 10^{-4} mv, there is a return to step 2 and the cycle is repeated (with the standard values of $\delta x = 0.05$ cm, $\delta t = 0.01$ msec, it was usually necessary to go back to step 2 two or three times). Otherwise, this time step is finished.

The results of a representative computation, illustrating the response to a short strong stimulus (about 2 times threshold) are plotted in Fig. 2. Because of the symmetry about $x = 0$, a pair of impulses arises at the stimulating electrode and propagate away in both directions. One is impressed by how quickly, in response to a strong stimulus, the propagating impulse achieves a constant conduction velocity. The velocity, measured by the displacement of the inflection of the rising phase per unit time, is already within a fraction of a percent of its constant value immediately after the action potential at $x = 0$ has reached its maximum.

An empirical test of the accuracy with which the difference equation approximates the partial differential equation is made by comparing this solution (for some point far away from the stimulating electrode) with the uniform wave solution of equation (3) (Hodgkin and Huxley, 1952; FitzHugh and Antosiewicz, 1959). The two waveforms superimpose (within the accuracy of the plots) over most of this time course; that is, they agree well in peak amplitude (90.5 mv) and duration, but a slight discrepancy (depending on the spatial integration interval, δx) can be seen in the exponentiation rate in the foot of the rising phase. Comparison of the predicted conduc-

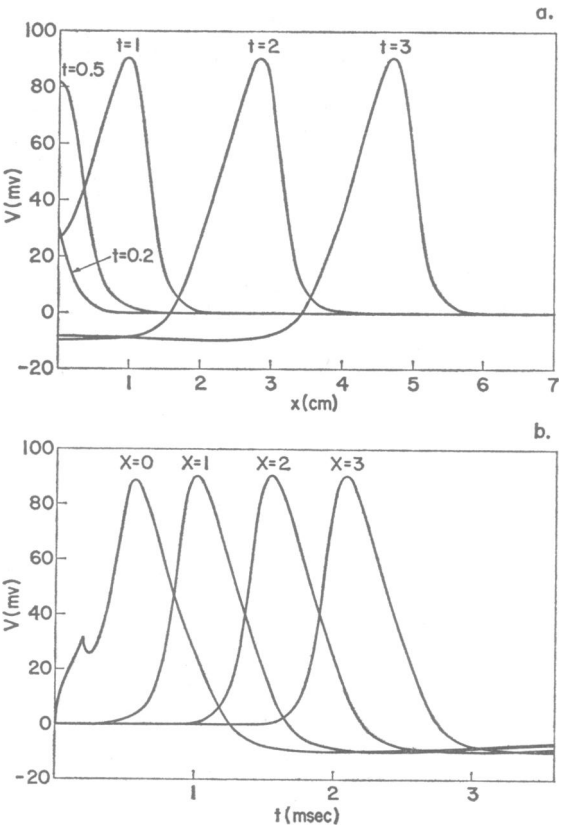

FIGURE 2 Computed response of the Hodgkin-Huxley axon to an 0.2 msec long stimulus of 10 μa (about 1.5 threshold) plotted as V against x for various times (*a.*) and as V against t for various distances (*b.*) 18.5° C. Integration parameters, $\delta x = 0.05$ cm, $J\delta x = 5$ cm, $\delta T = 0.01$ msec.

tion velocities provides a more sensitive test. These results are summarized in Table I. These results comfirm the general expectation that the finite-difference approximation should become more accurate as δx is made smaller. In addition, a temporal integration interval (δt) at least as large as 0.01 msec appears to give sufficient accuracy, since a value one fifth as large has practically no effect on the solution.

RESULTS AND DISCUSSION

The Threshold Strength-Duration Curve. The minimum intensity of stimulating current (I_s) required to initiate a propagating impulse has been estimated for several stimulus durations (t_s). Because each test stimulus required about 3 min of computing time simply to determine whether the axon had fired, we were satisfied to estimate the threshold stimulus as the mean between super- and sub-

TABLE I

CONDUCTION VELOCITY (θ) AT 18.5°C AND THE SPACE CONSTANT OF THE FOOT OF THE PROPAGATING ACTION POTENTIAL (λ') DETERMINED FOR SEVERAL VALUES OF THE INTEGRATION PARAMETERS

δx	δt	θ	λ'
cm	*msec*	*m/sec*	*cm*
0.05	0.01	18.694	−0.175
0.05	0.002	18.692	
0.025	0.01	18.724	−0.172
0.0125	0.01	18.732	
Uniform wave assumption (equation 2)		18.743396	−0.1692

threshold values differing by less than 1%. The results for two temperatures are given in Table II.

These theoretical predictions conform well to the empirical generalizations that for short duration stimuli the threshold is satisfied by a minimum quantity of charge, i.e. $I_s \cdot t_s \rightarrow Q_0$, whereas for long duration stimuli the threshold intensity asymptotically approaches a minimum value, the rheobase (I_0).

The threshold strength-duration relation for the space-clamped theoretical axon has been determined previously by Cole et al. (1955) and FitzHugh and Antosiewicz (1959). A simple basis for normalizing and comparing the various computational results is not at all obvious in the nonlinear processes described by the Hodgkin-Huxley model. However, such a basis is provided (Cole et al., 1955) by the classical phenomenological theories of excitation, in particular, the "two real time-factor" theories variously formulated by Hill, Rashevsky, and Monnier. Consideration of the classical theories may be justified by the fact that they quite accurately describe

TABLE II

THRESHOLD STIMULI ESTIMATED AS THE AMPLITUDE OF A RECTANGULAR PULSE OF CURRENT (I_s) OF DURATION (t_s) AT TEMPERATURES OF 6.3°C AND 18.5°C.

t_s	I_s		
msec	*6.3°C*	*μa*	*18.5°C*
0.05	34.6		26.4
0.1	17.6		13.4
0.2	8.94		7.13
0.5	3.76		3.33
1.0	2.06		2.07
2.0	1.238		1.57
4.0	0.887		
∞	0.823		1.53

experimental data. In Hill's formulation, an effective time constant for excitation (τ) is defined by

$$\tau = Q_0/I_0$$

and all possible threshold strength-duration curves are bounded by the limiting forms

$$I_s/I_0 = 1\Big/\left[1 - \exp\left(-\frac{\tau_s}{\tau}\right)\right] \tag{21}$$

and

$$I_s/I_0 = 1\Big/\left[\frac{\tau_s}{\tau}\exp\left(-\frac{\tau_s}{e\tau}\right)\right]. \tag{22}$$

The present results for the continuous (cable model) axon and the previous results for the space-clamped axon are compared with equations (21) and (22) in Fig. 3. From the comparison we observe that the continuous theoretical axon conforms more closely to the classical theory than does the space-clamped axon, but in both cases, the deviations are small. As shown by the normalizing factors, the effective time constant for excitation (τ) at a given temperature is significantly faster in the case of the continuous axon. This result is explained by the fact that the continuous

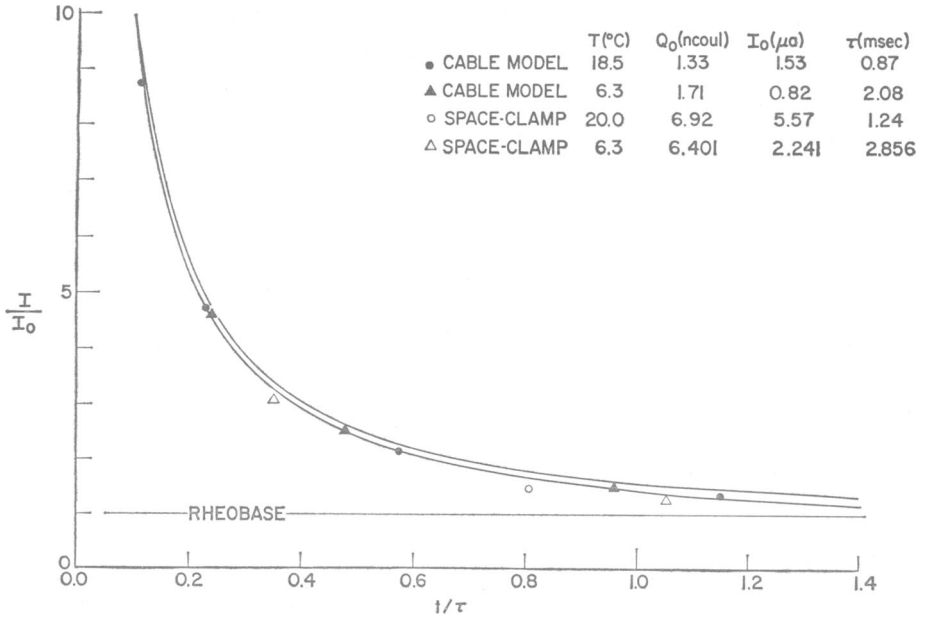

FIGURE 3 Comparison of the strength-duration relations of the theoretical axon for both the continuous (cable model) axon and for the space-clamped axon, with the limiting forms of the strength-duration curves predicted by the classical "two real-time factor" theories, equations (21) and (22).

axon requires a somewhat larger depolarization at the stimulating electrode in order to compensate for the electrical load of adjacent passive cable, and as a consequence of the greater depolarization the permeability changes underlying excitation occur more rapidly.

The effect of temperature on the excitability of the continuous axon was examined in greater detail by determining the threshold intensity for a brief (50 μsec) stimulus and for rheobase at several different temperatures. As shown in Fig. 4, the

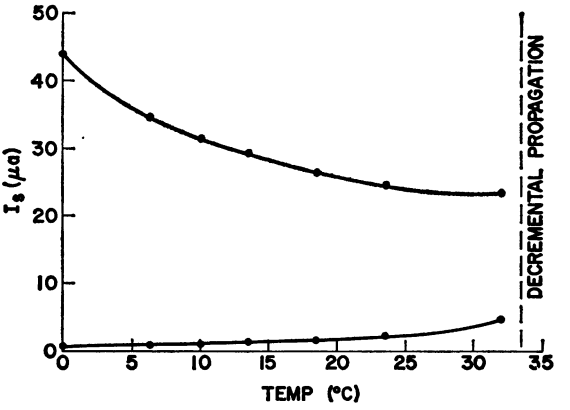

FIGURE 4 Temperature dependence of threshold stimulating current I_s. The short-shock (0.05 msec) threshold decreases monotonically (upper curve) while the rheobase (lower curve) increases with temperature.

equations predict that the short-shock threshold decreases monotonically with temperature whereas the rheobase increases with temperature. From solutions of the model under the uniform wave assumption (equation 3), Huxley (1959*a*) found that the theoretical axon was incapable of uniformly propagating an impulse at temperatures above 33.5°C.

For the space-clamped theoretical axon, FitzHugh (1966) has found that the rheobase increases with temperature, but that the short-shock threshold follows a shallow U-shaped curve with the optimum temperature at about 15°C. Recent experimental measurements show substantial qualitative agreement with the theoretical predictions. Guttman (1966) has measured the excitability of an axon under the space-clamp constraint and found that the rheobase increases with temperature, and that for short shocks the data suggest, but do not establish, an optimum temperature; on the other hand, Sjodin and Mullins (1958) observed that for 1 msec duration stimuli applied to a continuous axon, the threshold decreased monotonically with temperature.

Repetitive Firing of the Continuous Axon. Cole et al. (1955) have shown that the space-clamped theoretical axon will generate an indefinitely long train of

impulses in response to a constant current of sufficient intensity. Repetitive firing is of particular interest as an analogue for that part of various sensory receptors which transduce a slow generator potential into frequency of impulses in the sensory axon. Whereas the sensory transducer can often modulate the frequency over a hundred to one range, the space-clamped squid axon has only a very narrow range of about three to one (FitzHugh, 1961; Frankenhaeuser and Vallbo, 1965). We were, therefore, interested in seeing what effect the cable properties might have on the repetitive firing.

The partial differential equation was solved for step stimuli of various amplitudes, and representative solutions are plotted in Fig. 5 as the voltage response at the

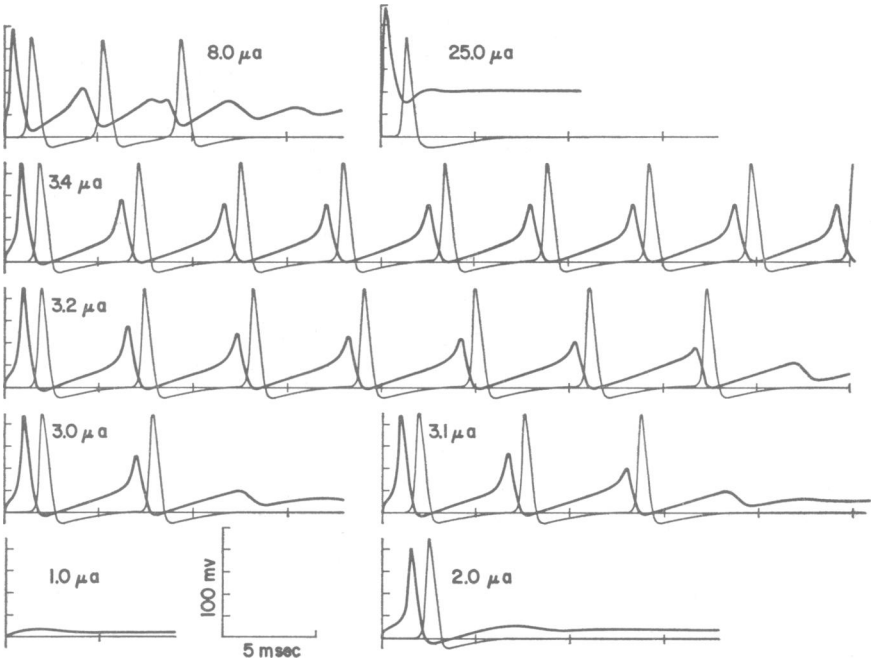

FIGURE 5 Response of the continuous axon to a steady stimulus of various intensities showing time course of the membrane potential V at $x = 0$ (heavy lines) and at $x = 2$ cm (lighter lines).

stimulating electrode (heavy curves) and at 2 cm away. The most striking result is that over the range of stimulus intensities which yield repetitive, propagating impulses, there is practically no modulation of the frequency of impulses. Indeed, if we compare the records at the extremes of this range, we see that the interval between impulses for 8.0 μa is only 30% less than that for 3.2 μa. Thus, when the cable properties are considered, the theoretical squid axon appears to be even less adequate as a model for the impulse transducing region of a sensory axon.

The computed result for the strongest stimulus shows that the theoretical axon, like a real axon, does not fire a burst of impulses in response to the intense depolarization at a cut end of the axon.

Initiation of a Subthreshold Propagating Wave. Huxley (1959*b*) demonstrated that the second order differential equation (3) obtained by assuming uniform propagation of a wave has two solutions in addition to the normal impulse. These solutions correspond to a single small wave and an indefinitely long series of oscillations propagating at much lower velocities than the normal impulse. It was presumed that these responses represent borderline cases between a superthreshold response and the local subthreshold response observable at a stimulating electrode. As such, it was expected that they would be very unstable.

To investigate these points we have solved the continuous axon model for the initial conditions that the resting axon is stimulated by brief (0.2 msec) pulses of current whose intensity was successively adjusted to converge to the threshold value. Some typical results are plotted in Fig. 6, where each set of curves shows the responses to a pair of stimuli bracketing the threshold by about $\pm 0.7\%$ in A, $\pm 0.007\%$ in *B*, and $\pm 0.7 \times 10^{-6}\%$ in *C*. For conditions *A* and *B* we see that the superthreshold and subthreshold responses measured at the stimulating electrode ($x = 0$) are readily distinguishable. When the stimulus is closer to threshold (B), we see that the latency between the stimulus and the superthreshold response is longer, and the amplitude of the superthreshold response at $x = 0$ is smaller. Approaching threshold (C), to the limit imposed by using single-precision floating point numbers with eight significant figures, we see that the superthreshold and subthreshold responses measured at the stimulating electrode and at 1 cm away superimpose over most of their time courses. The common waveform measured at 1 cm closely resembles the slow wave found by Huxley. With the precision employed for these computations, this slow wave does not propagate very far; the two solutions have greatly diverged at 2 cm, the superthreshold response there being only slightly smaller than the normal impulse.

These computations show that a slow subthreshold wave would be initiated, in principle, by a threshold stimulus. Furthermore, they give an impression that the slow wave is so unstable that we cannot expect to observe it experimentally. Leaving aside such difficult questions as to the effect of nonuniformity of axon geometry or membrane characteristics, this conclusion may be justified simply by considering the electrical noise observed in a real axon. The effect of this noise is to cause apparently random fluctuation of the threshold. Thus, if one measures the probability of firing as a function of stimulus intensity, one obtains a density function that is approximately Gaussian with a standard deviation of about 1%. On this basis alone, one could expect to observe responses as close to threshold as Fig. 6B only rarely in a long series of tests, and the probability of seeing responses like Fig. 6C would be nil.

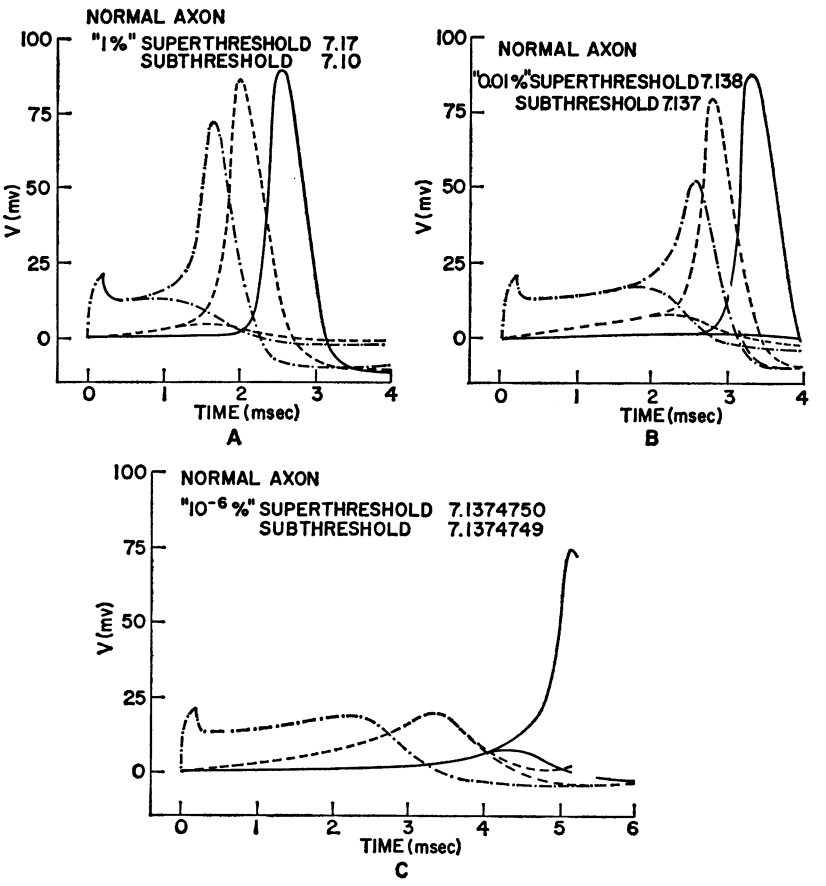

FIGURE 6 Response of continuous axon to super- and subthreshold stimuli of 0.2 msec duration for various amplitudes converging towards threshold. Time courses of V at $x = 0$, 1, and 2 cm are plotted.

A rigorous mathematical test for the stability of the propagating waves has not yet been developed. However, we can gain some insight into the highly unstable behavior by considering the characteristic relation between the ionic current and membrane potential in the voltage-clamp experiments (Hodgkin, Huxley, and Katz, 1952, p. 439). At short times $\partial I_i/\partial V$ is negative and large at that value of membrane potential corresponding to the amplitude of the subthreshold wave. This relation means that a small depolarizing perturbation of the wave would cause (a short time later) a large increase in inward ionic current which would act to regenerate that perturbation, with the result that the wave would "flip" over to the normal stable impulse. On this basis we would expect that any agent which reduced $\partial I_i/\partial V$, say by generally reducing the inward component of I_i, would correspondingly lessen the

degree of instability of the subthreshold wave. Hence, we were led to consider the effects of local anesthetics on the initiation of the unstable waves.

Effects of an Anesthetic Agent on Excitation and Propagation. Voltage-clamp studies have shown that local anesthetics, such as procaine and alcohol, exert their narcotizing action by reducing $\bar{g}_{Na}$ (usually $\bar{g}_K$ is also reduced, but typically not as much as $\bar{g}_{Na}$) without otherwise affecting the kinetics of the conductance changes (Taylor, 1959; Moore et al., 1964; Moore, 1958; Armstrong and Binstock, 1964). To examine the effects of such agents on excitability, we have done some computations for the condition that both $\bar{g}_{Na}$ and $\bar{g}_K$ were attenuated by the same factor (η), and $\bar{g}_L$ and V_L were adjusted so that both the resting membrane potential and resting conductance were held constant. To determine the range of η in which the axon would be capable of propagating a uniform wave, equation (3) was solved for several values of η. The results of these computations are summarized in Fig. 7 where the conduction velocity (θ) and the amplitude of the uniformly propagated

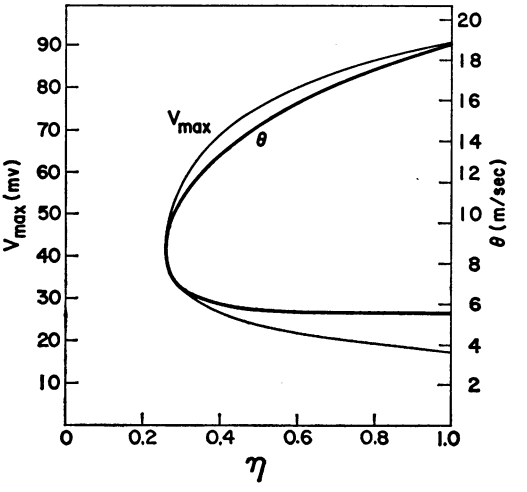

FIGURE 7 Peak amplitude of the propagated impulse (V_{max}) and conduction velocity (θ) plotted as functions of attenuation factor of the ionic conductances η.

impulse (V_{max}) are plotted as functions of η. The upper limbs of each curve correspond to the normal (stable) impulse, and the lower limbs correspond to the subthreshold (unstable) wave solutions; the differences in θ between the two types of subthreshold waves cannot be resolved on the scale of this plot. Except for the fact that we made small adjustments of $\bar{g}_L$ and V_L, the curve of θ versus η could have been deduced from the dimensional considerations of Huxley (1959*a*).

From Fig. 7 we see that there are no uniform wave solutions for η less than 0.261, and we expect only decrementally propagated responses, if any, for small η. An example of this is illustrated in Fig. 8A, in which the partial differential equation

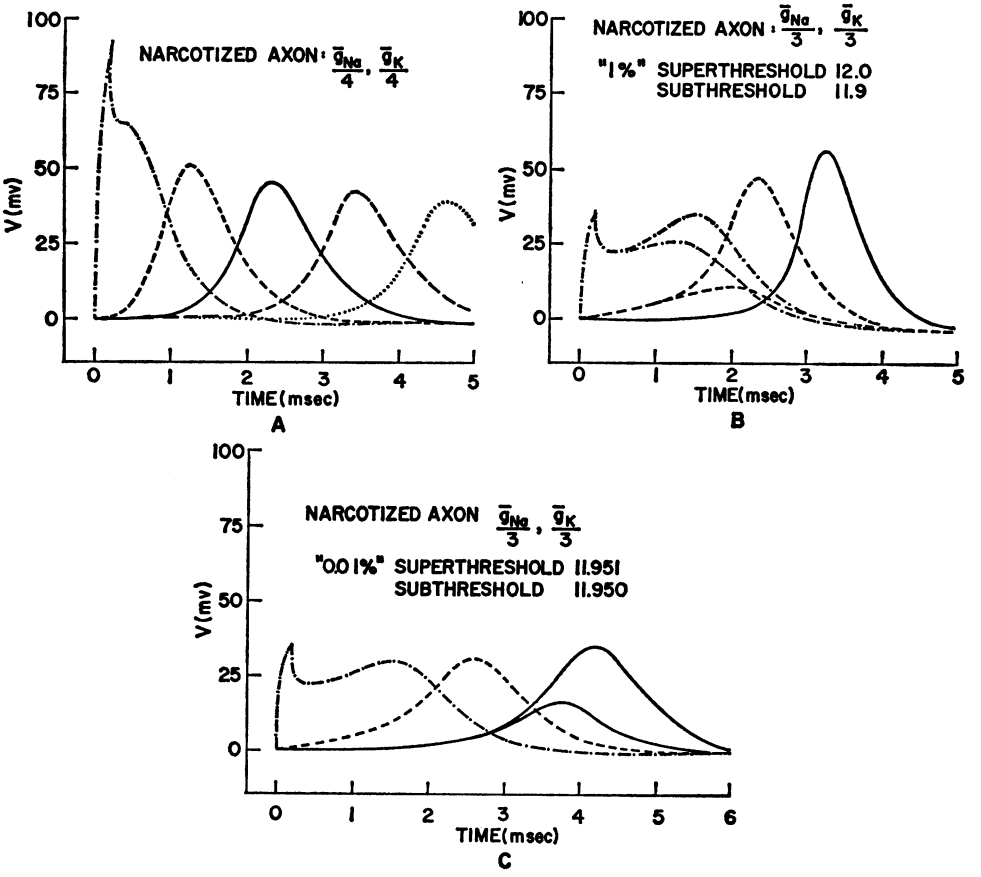

FIGURE 8 A Decrementally propagated impulse resulting from attenuation of $\bar{g}_{Na}$ and $\bar{g}_K$ to ¼ their normal values. Plotted as V against t for $x = 0$, 1, 2, 3, and 4 cm. A very strong stimulus was applied at $x = 0$. B and C: Super- and subthreshold response of the axon when $\bar{g}_{Na}$ and $\bar{g}_K$ have been attenuated to ⅓ their normal values. Plotted as V against t for $x = 0$, 1, and 2 cm. The curve at $x = 1$ cm in part C illustrates the unstable wave under these conditions.

was solved for $\eta = 0.25$. A somewhat surprising result from this computation is the slow rate of decrement under this condition; indeed, the response to a strong stimulus is still some 40 mv in amplitude at 4 cm away from the stimulating electrode.

For a lesser degree of narcotization, say $\eta = 0.33$ for example, the axon is capable of uniformly propagating both a stable and an unstable wave, which can easily be distinguished, the stable wave being about 60 mv in amplitude with a conduction velocity of 12 m/sec and the unstable wave being about 30 mv with a velocity of 6 m/sec. Solutions of the partial differential equation for $\eta = 0.33$, illustrating responses near threshold, are shown in Fig. 8B and C. In Fig. 8C we

see that the responses to super- and subthreshold stimuli differing by one part in 10^4 are indistinguishable at 1 cm away from the stimulating electrode, and that this waveform corresponds quite well in amplitude and velocity to the unstable wave solution. This result suggests that under an appropriate degree of narcotization the subthreshold propagating wave might be experimentally observable.

Received for publication 4 January 1966.

REFERENCES

ARMSTRONG, C. M., and BINSTOCK, L., 1964, *J. Gen. Physiol.*, **48**, 265.
COLE, K. S., ANTOSIEWICZ, H. A., and RABINOWITZ, P., 1955, *J. Soc. Indust. and Appl. Math.*, **3**, 153.
DODGE, F. A., and FRANKENHAEUSER, B., 1958, *J. Physiol.*, **143**, 76.
FITZHUGH, R., 1961, *Biophysic. J.*, **1**, 445.
FITZHUGH, R., 1962, *Biophysic. J.*, **2**, 11.
FITZHUGH, R., and ANTOSIEWICZ, H. A., 1959, *J. Soc. Indust. and Appl. Math.*, **7**, 447.
FITZHUGH, R., 1966, *J. Gen. Physiol.*, **49**, 989
FRANKENHAEUSER, B., and VALLBO, A. B., 1965, *Acta Physiol. Scand.*, **63**, 1.
GUTTMAN, R., 1966, *J. Gen. Physiol.*, **49**, 1007.
HODGKIN, A. L., and HUXLEY, A. F., 1952, *J. Physiol.*, **117**, 500.
HODGKIN, A. L., HUXLEY, A. F., and KATZ, B., 1952, *J. Physiol.*, **116**, 424.
HUXLEY, A. F., 1959*a*, *Ann. New York Acad. Sc.*, **81**, 221.
HUXLEY, A. F., 1959*b*, *J. Physiol.*, **148**, 80.
MOORE, J. W., ULBRICT, W., and TAKATA, M., 1964, *J. Gen. Physiol.*, **48**, 279.
MOORE, J. W., 1958, *Fed. Proc.*, **17**, 113.
SJODIN, R. A., and MULLINS, L. J., 1958, *J. Gen. Physiol.*, **42**, 39.
TAYLOR, R. E., 1959, *Am. J. Physiol*, **196**, 1071.